Calculation of the dynamic first electronic hyperpolarizability β(−ωσ; ω1, ω2) of periodic systems. Theory, validation, and application to multi-layer MoS2

Lorenzo Maschio, Michel Rérat, Bernard Kirtman, and Roberto Dovesi

Citation: The Journal of Chemical Physics **143**, 244102 (2015); doi: 10.1063/1.4937770
View online: http://dx.doi.org/10.1063/1.4937770
View Table of Contents: http://scitation.aip.org/content/aip/journal/jcp/143/24?ver=pdfcov
Published by the AIP Publishing

Calculation of the dynamic first electronic hyperpolarizability $\beta(-\omega_\sigma; \omega_1, \omega_2)$ of periodic systems. Theory, validation, and application to multi-layer MoS_2

Lorenzo Maschio,[1,a)] Michel Rérat,[2] Bernard Kirtman,[3] and Roberto Dovesi[1]
[1]*Dipartimento di Chimica and NIS (Nanostructured Interfaces and Surfaces) Centre, Università di Torino, via Giuria 5, I-10125 Torino, Italy*
[2]*Equipe de Chimie Physique, IPREM UMR5254, Université de Pau et des Pays de l'Adour, 64000 Pau, France*
[3]*Department of Chemistry and Biochemistry, University of California, Santa Barbara, California 93106, USA*

(Received 6 August 2015; accepted 27 November 2015; published online 22 December 2015)

We describe our implementation of a fully analytical scheme, based on the 2n + 1 rule, for computing the coupled perturbed Hartree Fock and Kohn-Sham dynamic first hyperpolarizability tensor $\beta(-\omega_\sigma; \omega_1, \omega_2)$ of periodic 1D (polymer), 2D (slab), and 3D (crystal) systems in the CRYSTAL code [R. Dovesi *et al.*, Int. J. Quantum Chem. **114**, 1287 (2014)], which utilizes local Gaussian type basis sets. The dc-Pockels (dc-P) and second harmonic generation (SHG) tensors are included as special cases. It is verified that (i) symmetry requirements are satisfied; (ii) using LiF as an example, the infinite periodic polymer result agrees with extrapolated finite oligomer calculations and, likewise, for the build-up to a 2D slab and a 3D crystal; (iii) the values converge to the static case for low frequencies; and (iv) the Bishop-deKee dispersion formulas relating dc-P, SHG, and general processes are reproduced through quartic terms. Preliminary SHG calculations on multi-layer MoS_2 satisfactorily reproduce experimental data. © *2015 AIP Publishing LLC.* [http://dx.doi.org/10.1063/1.4937770]

I. INTRODUCTION

There continues to be considerable interest in the nonlinear optical (NLO) properties of materials, motivated by fundamental as well as practical considerations. These properties have been useful and they remain potentially useful for a wide variety of optical and photonic applications.[1–4] The materials studied range broadly from small molecules to large complex bio- and nano-systems. Past and on-going developments in this field have been fueled by a combination of experiment and theory. Our own focus has been on the theoretical/computational aspect, especially for systems that are either periodic or may be modeled as such.

For periodic systems, the opportunity to exploit translational symmetry provides major computational advantages. On the other hand, a problem arises as to how to properly express the term that describes the electronic dipole interaction with a spatially homogeneous external electric field (or fields), $\vec{\mathcal{E}}$, which is the origin of the various NLO processes. The conventional scalar interaction potential used in the molecular context,

$$\hat{V}(\vec{r}) = \vec{\mathcal{E}} \cdot \vec{r}, \tag{1}$$

is unsuitable for periodic systems since it breaks translational symmetry and, in addition, it is unbounded. Here, $\vec{r}$ is the electronic position operator and the electronic charge has been taken as $e = -1$ a.u.

Beginning a little over 20 years ago, substantial advances with regard to the proper definition of the interaction operator have been made. Two different formulations for static fields, that preserve translational symmetry, were presented by Resta[5] and by King-Smith and Vanderbilt (KSV).[6] Subsequently, for periodic polymers in particular, two time-dependent approaches were introduced, one based on the vector potential[7] and the other on subtracting out the non-periodic part of the scalar potential.[8] These time-dependent formulations are equivalent to one another[7] and, in the static field limit, reduce to the KSV expression.[9] Ferrero *et al.*[10,11] extended the 1D vector potential treatment of polymers to 2D and 3D but, as in Refs. 5 and 6, considered only the static limit in their implementation. For homogeneous electric fields, which may be either time-dependent or not, the general expression in 1-, 2-, or 3-D that replaces Eq. (1) becomes

$$\imath\vec{\mathcal{E}} \cdot e^{\imath\vec{k}\cdot\vec{r}}\vec{\nabla}_k e^{-\imath\vec{k}\cdot\vec{r}} = \sum_b \mathcal{E}_b \hat{\Omega}^{(\mathcal{E}_b)}(\vec{k}), \tag{2}$$

where $\vec{k}$ is a reciprocal space vector, $\hat{\Omega}^{(\mathcal{E}_b)}(\vec{k})$ refers to the b component of the gradient vector, and $\mathcal{E}_b = \mathcal{E}_b(t)$ is the b component of the time-dependent incident electric field or fields. The operator in Eq. (2) is clearly diagonal in k space; it is valid for all materials as long as they have a non-zero bandgap.

NLO properties are defined in terms of a power series expansion in the various electric fields. An appropriate expansion may be obtained most conveniently by means of perturbation theory. Indeed, the time-dependent polymer treatments mentioned above were developed in the context of coupled perturbed Hartree-Fock (CPHF) theory as was the implementation for static fields acting on periodic systems of 1, 2, and 3 dimensions carried out by Ferrero *et al.*,[10,11] within the CRYSTAL program.[12,13] Both first and second static hyperpolarizabilities are computed in CRYSTAL by means of the 2n + 1 rule. In addition to CPHF, coupled perturbed Kohn-Sham (CPKS) calculations[14,15] using gradient corrected and hybrid functionals are also available. The CRYSTAL code

a)lorenzo.maschio@unito.it

that employs local Gaussian-type basis functions is efficiently parallelized and takes maximum advantage of symmetry (see Ref. 16 and references therein) so that large unit cells are tractable.

Frequency-dependent linear polarizabilities are available in CRYSTAL, and in many other programs as well (e.g., ADF-Band, Yambo, EXCITING, Wien2k *et al.*). However, neither CRYSTAL nor, to our knowledge, any other code has implemented a fully periodic coupled perturbation theory treatment of dynamic (i.e., frequency-dependent) NLO properties until this work, so that the state-of-the-art treatment of crystalline systems has been until now the use of molecular embedding techniques, when possible.[17]

In the present paper, we develop and test a fully analytical CPHF/CPKS code for the general dynamic $\beta(-\omega_\sigma;\omega_1,\omega_2)$ tensor based on the $2n+1$ rule, which has now been implemented in the CRYSTAL program.[12,13] The dc-Pockels (dc-P) and second harmonic generation (SHG) tensors, $\beta(-\omega;\omega,0)$ and $\beta(-2\omega;\omega,\omega)$, are included, of course, as special cases. For CPKS, the adiabatic approximation was utilized.

As part of the vetting, it was verified that the various symmetry relations between the components of $\beta(-\omega_\sigma;\omega_1,\omega_2)$ are obeyed. Moreover, as in the case of static first hyperpolarizabilities, the consistency of the 0D, 1D, 2D, and 3D treatments was established using LiF units to build-up from a single molecule to finite linear chains and, then, to infinite chains, slabs, and, finally, FCC LiF. In all structures, one atom was slightly displaced with respect to its equilibrium position in order to yield nonvanishing values—see Section III and Figure 1. The convergence behavior with respect to the number of $\vec{k}$ points, as well as the parameters controlling the truncation of the coulomb and exchange series that enter into both the zero field SCF calculation and the first-order perturbation treatment, were also studied.

As a first application of the method, we have computed SHG properties of multi–layer MoS_2 structures. Our results correctly reproduce the strong decay of the SHG intensity with the (odd) number of stacked layers.

In Sec. II, the pertinent theoretical background is presented. Then, in Sec. III we report on the checks that were carried out. These include symmetry behavior, build-up from 0D to 3D, and the relationship between different properties for the frequency-dependence of the diagonal components. The effect of the various computational parameters on accuracy and numerical stability is also considered. In Sec. IV, we report our results for MoS_2 nanostructures. Finally, Sec. V provides an overall summary and some directions of future work.

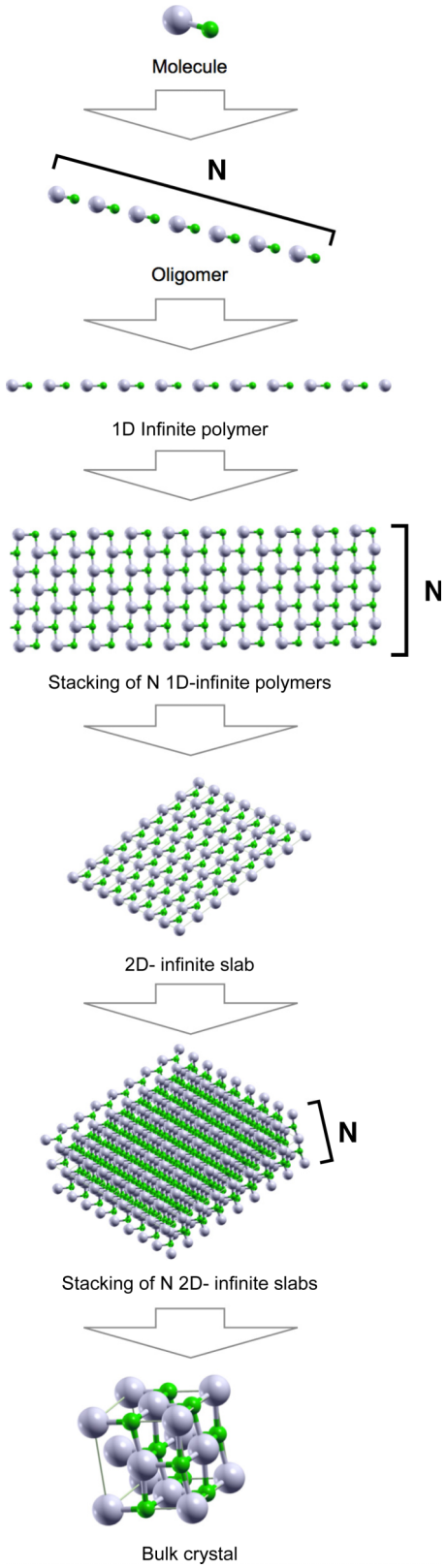

FIG. 1. Buildup of LiF structures from 0D to 3D, used as test systems in this work as discussed in Section III B 1.

II. COUPLED PERTURBED HF/KS CALCULATION OF THE DYNAMIC FIRST HYPERPOLARIZABILITY

In order to derive our $2n+1$-rule working formula for the dynamic first hyperpolarizability of a 3D periodic system given by Eq. (3) below, we start with the expression for the static limit due to Ferrero *et al.* (see Eq. (58) in Ref. 18). This expression has exactly the same form as that shown below except, of course, that all frequencies are set equal to zero. The 3D static result was obtained, in fact, by generalizing the 1D periodic frequency-dependent treatment of Kirtman *et al.*[7] which, in turn, was based on the time-dependent Hartree-Fock formulation for molecules developed

by Karna and Dupuis[19] (KD). Thus, we use KD to introduce the frequency-dependence. They considered just four special cases (see Table VII in Ref. 19), including static, and their treatment pertains only to the first two terms in square brackets below. Nonetheless, it is straightforward to generalize their formulation as we have done. Finally, the use of the operator $P_{\frac{t}{-\omega_\sigma},\frac{u}{+\omega_1},\frac{v}{+\omega_2}}$ which permutes the pairs $(t/-\omega_\sigma)$, $(u/+\omega_1)$, and $(v/+\omega_2)$ has been discussed, for example, by Bishop.[20] From the approach just described, the general expression for the first hyperpolarizability of closed-shell periodic systems in the presence of frequency-dependent fields may be written as

$$\beta_{tuv(-\omega_\sigma;\omega_1,\omega_2)} = -\frac{2}{n_k}\mathcal{K}_{-\omega_\sigma,\omega_1,\omega_2}\sum_{\vec{k}}\Re\sum_i\sum_a P_{\frac{t}{-\omega_\sigma},\frac{u}{+\omega_1},\frac{v}{+\omega_2}} \times\left\{U^{(t)*}_{ai(-\omega_\sigma)}(\vec{k})\left[\sum_b G^{(u)}_{ab(+\omega_1)}(\vec{k})U^{(v)}_{bi(+\omega_2)}(\vec{k}) - \sum_j U^{(v)}_{aj(+\omega_2)}(\vec{k})G^{(u)}_{ji(+\omega_1)}(\vec{k}) + \imath\frac{\partial U^{(v)}_{ai(+\omega_2)}(\vec{k})}{\partial k_u}\right]\right\}, \quad (3)$$

where i,j and a,b run over occupied and virtual crystalline orbitals (CO), respectively, t,u,v indicate directions of the field, and $\omega_\sigma = \omega_1 + \omega_2$. The last term of Eq. (3) only appears for infinite periodic systems described under the Born-von-Karman condition. A working expression is developed in Appendix A.

In Eq. (3), the coefficient $\mathcal{K}_{-\omega_\sigma;\omega_1,\omega_2}$ depends on the nonlinear optical process[21] ($\mathcal{K}_{0,0,0} = 1$, $\mathcal{K}_{-2\omega,\omega,\omega} = 1/2$, $\mathcal{K}_{-\omega,0,\omega} = 2$, $\mathcal{K}_{0,\omega,-\omega} = 1/2$, $\mathcal{K}_{\omega,-2\omega,\omega} = 1$, and $\mathcal{K}_{-\omega_\sigma,\omega_1,\omega_2} = 1$ if neither ω_σ, nor ω_1 nor ω_2 are null). The off-diagonal virt-occ blocks of the perturbation matrix $U^{(u)}_{ai(+\omega_1)}(\vec{k})$ are defined as (the diagonal blocks are chosen to vanish in the non-canonical KD treatment),

$$U^{(u)}_{ai(+\omega_1)}(\vec{k}) = -\frac{G^{(u)}_{ai(+\omega_1)}(\vec{k})}{\mathbb{E}_a(\vec{k}) - \mathbb{E}_i(\vec{k}) + \omega_1}. \quad (4)$$

Here, the $G^{(u)}_{ai(+\omega_1)}(\vec{k})$ matrix is obtained after Fourier transformation of the first-order atomic orbital (AO) Fock matrix as

$$G^{(u)}_{ai(+\omega_1)}(\vec{k}) = \Xi_{ai}(\vec{k}) + \sum_{\mu,\nu}\left[C^*_{\mu a}(\vec{k})F^{(u)}_{\mu,\nu(+\omega_1)}(\vec{k})C_{\nu i}(\vec{k})\right], \quad (5)$$

where $\Xi_{ai}(\vec{k}) = \langle a(\vec{k})|r + \imath\nabla_{\vec{k}}|i(\vec{k})\rangle = \mathcal{Z}_{ai}(\vec{k}) + \imath\mathcal{Q}_{ai}(\vec{k})$ is the transition moment operator between occupied $i(\vec{k})$ and virtual $a(\vec{k})$ crystalline orbitals.[8,22] $F^{(u)}_{\mu,\nu(+\omega_1)}(\vec{k})$, in turn, is determined using the perturbed density $D^u_{\rho,\tau\vec{n}(+\omega_1)}$,

$$F^{(u)}_{\mu,\nu(+\omega_1)}(\vec{k}) = \sum_{\vec{g}} e^{-\imath\vec{k}\cdot\vec{g}}\sum_{h,n}\sum_{\rho,\tau}\left(\mu\nu^{\vec{g}}||\rho^{\vec{h}}\tau^{\vec{h}+\vec{n}}\right)D^{(u)}_{\rho,\tau\vec{n}(+\omega_1)}, \quad (6)$$

with the density being obtained as a back-Fourier transform of its reciprocal space image, that—assuming integer occupation of all orbitals—is expressed for closed shells as

$$D^{(u)}_{\mu,\nu\vec{g}(+\omega_1)} = 2\sum_{\vec{k}} e^{\imath\vec{k}\cdot\vec{g}}\left[\sum_{ia} C_{\mu a}(\vec{k})\,U^{(u)}_{ai(+\omega_1)}(\vec{k})\,C^*_{\nu i}(\vec{k}) + \sum_{ia} C_{\mu i}(\vec{k})\,U^{(u)*}_{ia(+\omega_1)}(\vec{k})C^*_{\nu a}(\vec{k})\right]. \quad (7)$$

As a result, $G^{(u)}_{ai(+\omega_1)}(\vec{k})$ ultimately depends on $U^{(u)}_{ai(+\omega_1)}(\vec{k})$ which, in turn, depends on $G^{(u)}_{ai(+\omega_1)}(\vec{k})$.

Hence, a self-consistent procedure must be employed to obtain the $U^{(u)}(\vec{k})$ matrix in Eq. (4). This procedure has been adopted in a previous work[18] for periodic systems at the static ($\omega_\sigma = \omega_1 = \omega_2 = 0$) limit.

The expression for the density functional theory (DFT) contribution to $\beta_{tuv}(-\omega_\sigma;\omega_1,\omega_2)$ is obtained from the expression for the corresponding static property as reported in Eq. (20) of Ref. 15,

$$\begin{aligned}\beta^{DFT}_{tuv}(-\omega_\sigma;\omega_1,\omega_2) = \sum_i w_i\hat{P}_{t/-\omega_\sigma,u/+\omega_1,v/+\omega_2}\Bigg[&\frac{\partial^3 f^{XC}}{\partial\rho^3}\rho^t_{(-\omega_\sigma)}\rho^u_{(+\omega_1)}\rho^v_{(+\omega_2)} + 2\frac{\partial^3 f^{XC}}{\partial\rho^2\partial\mid\nabla\rho\mid^2}\left(\rho^t_{(-\omega_\sigma)}\rho^u_{(+\omega_1)}\nabla\rho\cdot\nabla\rho^v_{(+\omega_2)}\right)\\ &+4\frac{\partial^3 f^{XC}}{\partial\rho\partial(\mid\nabla\rho\mid^2)^2}\left(\rho^t_{(-\omega_\sigma)}\nabla\rho\cdot\nabla\rho^u_{(+\omega_1)}\nabla\rho\cdot\nabla\rho^v_{(+\omega_2)}\right)\\ &+8\frac{\partial^3 f^{XC}}{\partial(\mid\nabla\rho\mid^2)^3}\nabla\rho\cdot\nabla\rho^t_{(-\omega_\sigma)}\nabla\rho\cdot\nabla\rho^u_{(+\omega_1)}\nabla\rho\cdot\nabla\rho^v_{(+\omega_2)} + 2\frac{\partial^2 f^{XC}}{\partial\rho\partial\mid\nabla\rho\mid^2}\left(\rho^t_{(-\omega_\sigma)}\nabla\rho^u_{(+\omega_1)}\cdot\nabla\rho^v_{(+\omega_2)}\right)\\ &+4\frac{\partial^2 f^{XC}}{(\partial(\mid\nabla\rho\mid^2)^2}\left(\nabla\rho\cdot\nabla\rho^t_{(-\omega_\sigma)}\nabla\rho^u_{(+\omega_1)}\cdot\nabla\rho^v_{(+\omega_2)}\right)\Bigg]_{\mathbf{r_i}}. \end{aligned} \quad (8)$$

III. TESTING THE IMPLEMENTATION

In this section we aim at providing numerical evidence that (a) the symmetry of the β tensor is fully satisfied, (b) the formalism is consistent throughout 0D to 1D, 2D, and 3D periodic systems, (c) all the values of the dynamic tensors converge to the static value at long wavelength, and (d) the Bishop-De Kee dispersion formula[23,24] is satisfied. As in previous works on static CPHF/KS implementations,[11,25,26] we use LiF structures (see Figure 1) as a benchmark system, which we will describe in detail in Section III B 1.

A. Symmetry of the β tensor

Perhaps the simplest, and least stringent, test of our implementation is the symmetry of the β tensor, which requires that certain of the 27 components must be equal and others must vanish. These requirements differ depending upon the dimensionality.

(i) In 1D we take the periodic direction to be along x. Then, in general, for $\beta_{i,j,k}(-\omega_\sigma;\omega_1,\omega_2)$ all components with an odd-power of y and/or z vanish. Furthermore, y and z are equivalent directions so that $\beta_{xyy} = \beta_{xzz}$, $\beta_{yyx} = \beta_{zzx}$, and $\beta_{yxy} = \beta_{zxz}$. In addition, all simultaneous permutations of the frequencies and directions for the set $(\omega_\sigma/i,\omega_1/j,\omega_2/k)$ must yield the same value. In particular, we examined for second harmonic generation (SHG; $\omega_\sigma = 2\omega$, $\omega_1 = \omega_2 = \omega$) the permutation $\omega_1/j \leftrightarrow \omega_2/k$, which leads to $\beta_{yxy} = \beta_{yyx}$, whereas for the dc-Pockels effect (dc-P; $\omega_\sigma = \omega$, $\omega_1 = \omega$, $\omega_2 = 0$) the same permutation leads to $\beta_{yxy}(-\omega;\omega,0) = \beta_{yyx}(-\omega;0,\omega)$.

(ii) In 2D we consider (see Section III B 1 below) periodicity in the x,y plane with the x–direction being asymmetric and the y–direction symmetric. Then, again, the components of the β tensor with an odd power in y or z will be null. Now, however, y and z are inequivalent although the permutation $\omega_1/j \leftrightarrow \omega_2/k$ leads separately to the same relations as in (i) for z and y.

(iii) Finally, in 3D we add (see, again, Section III B 1 below) a symmetric periodic z direction so that y and z are, once again, equivalent. Then the symmetry requirements are the same as in (i).

All of the above symmetry relations have been successfully tested. In Table I, the full tensors obtained for some of the model systems described in Section III B 1 below, as computed at the Hartree-Fock level, are reported as an example.

TABLE I. Tensor elements for dc-Pockels and SHG dynamic β for the three periodic dimensionalities of (distorted) LiF model structures considered in the present work (cf. Figure 1). Symmetries of the tensors can be observed as discussed in Section III A. All values are in a.u. as obtained from Hartree-Fock calculations at $\omega = 200$ nm.

		dc-Pockels											
		Polymer			Slab			Bulk					
	v	x	y	z		x	y	z		x	y	z	
t	u												
	x	7.902 52	0.000 00	0.000 00	x	5.323 65	0.000 00	0.000 00	x	3.586 02	0.000 00	0.000 00	
x	y	0.000 00	−0.664 02	0.000 00	y	0.000 00	−0.299 43	0.000 00	y	0.000 00	−0.351 99	0.000 00	
	z	0.000 00	0.000 00	−0.664 03	z	0.000 00	0.000 00	−0.171 37	z	0.000 00	0.000 00	−0.351 87	
	x	0.000 00	−0.494 51	0.000 00	x	0.000 00	−0.129 25	0.000 00	x	0.000 00	−0.263 92	0.000 00	
y	y	−0.664 02	0.000 00	0.000 00	y	−0.299 47	0.000 00	0.000 00	y	0.351 98	0.000 00	0.000 00	
	z	0.000 00	0.000 00	0.000 00	z	0.000 00	0.000 00	0.000 00	z	0.000 00	0.000 00	0.000 00	
	x	0.000 00	0.000 00	−0.494 52	x	0.000 00	0.000 00	−0.112 95	x	0.000 00	0.000 00	−0.263 92	
z	y	0.000 00	0.000 00	0.000 00	y	0.000 00	0.000 00	0.000 00	y	0.000 00	0.000 00	0.000 00	
	z	−0.664 03	0.000 00	0.000 00	z	0.171 36	0.000 00	0.000 00	z	0.351 86	0.000 00	0.000 00	
		Second harmonic generation											
		Polymer			Slab			Bulk					
	v	x	y	z		x	y	z		x	y	z	
t	u												
	x	35.733 82	0.000 00	0.000 00	x	21.921 27	0.000 00	0.000 00	x	9.952 16	0.000 00	0.000 00	
x	y	0.000 00	−4.189 52	0.000 00	y	0.000 00	−4.583 16	0.000 00	y	0.000 00	−1.970 79	0.000 00	
	z	0.000 00	0.000 00	−4.189 72	z	0.000 00	0.000 00	−0.985 57	z	0.000 00	0.000 00	−1.970 92	
	x	0.000 00	2.529 78	0.000 00	x	0.000 00	−0.901 25	0.000 00	x	0.000 00	−0.815 50	0.000 00	
y	y	2.529 78	0.000 00	0.000 00	y	−0.901 25	0.000 00	0.000 00	y	−0.815 50	0.000 00	0.000 00	
	z	0.000 00	0.000 00	0.000 00	z	0.000 00	0.000 00	0.000 00	z	0.000 00	0.000 00	0.000 00	
	x	0.000 00	0.000 00	−0.494 52	x	0.000 00	0.000 00	0.208 34	x	0.000 00	0.000 00	−0.815 01	
z	y	0.000 00	0.000 00	0.000 00	y	0.000 00	0.000 00	0.000 00	y	0.000 00	0.000 00	0.000 00	
	z	−0.664 03	0.000 00	0.000 00	z	0.208 34	0.000 00	0.000 00	z	−0.815 01	0.000 00	0.000 00	

B. Build-up from molecule to 1-, 2-, and 3-D

1. The model systems

As mentioned in the Introduction, one key test that we considered is the evolution of the non-null components of β with increasing dimensionality of the system. For this purpose, n-dimensional LiF structures were built by assembling a finite number of (n − 1)-dimensional "monomers" progressively, as shown in Figure 1. Accordingly, we joined Li-F units (0D LiF) to form linear chains of increasing length (oriented along the x axis), that evolve to an infinite linear chain (1D LiF). Then, we arranged infinite linear chains next to each other in a plane by alternating Li and F ions along the growing direction (y axis) to form an infinite LiF layer (2D LiF). Finally, we superimposed LiF infinite layers to form slabs of growing thickness along the z direction to approximate bulk LiF (again, the stacking of planes is such that the alternation of Li and F ions along z is preserved).

In all cases, one of the Li atoms is at the origin. The a lattice parameter used in the 1-3D cases is that of bulk LiF (3D), i.e., 4.017 Å. If the Li-F distances (d_{Li-F}) are kept at $a/2$ (symmetric case, with equivalent Li-F and F-Li distances), all the elements of the first hyperpolarizability $\boldsymbol{\beta}$ tensor vanish by symmetry. For that reason the F ion at (0.5, 0.0, 0.0), in fractional units, was shifted to 0.45 along the x direction.

All calculations were performed with a basis set consisting of a 6-1 contraction (one s and one sp shell) for Li, and a 7-311(1) contraction for F (one s, 3sp, and one d shell). The exponents of the most diffuse shells are $\alpha^{sp}_{Li} = 0.525$, $\alpha^{sp}_{F} = 0.437$ and 0.137, $\alpha^{d}_{F} = 0.6$ bohr^{-2}. These geometries and the basis set are the same as used in previous papers in which our CPHF/KS implementation for the static polarizability tensor,[11] infrared intensities,[25] and Raman intensities[26] was presented.

2. Computational parameters

The sensitivity of our CPHF/KS implementation to the several computational parameters involved has been widely discussed for the static polarizability and hyperpolarizabilities.[10,11,18,25–27] Although there is no reason to suppose the behavior would be different in the present case, we cautiously adopted tighter values than would be thought necessary for the integral screening tolerances TOLINTEG keyword in Crystal $T1 = T2 = T3 = T4 = 10^{-10}$, $T5 = 10^{-20}$. Convergence on the HF or DFT energy in SCF cycles was set to 10^{-12} hartree.

Convergence for the first-order CPHF/KS cycles, which is determined by the linear polarizability α, was set to 10^{-6}. It should be noted that the convergence behavior of the first-order perturbation equations can be delicate depending upon the proximity of the frequency to the lowest resonance. Indeed, using the convergence accelerators implemented in Crystal (Anderson and Broyden schemes) led to premature convergence in some cases. Therefore, we refrained, in general, from using these schemes for the calculations presented herein. It is our intention to implement DIIS[28,29] in the near future.

3. Results for 0D → 3D buildup

The β tensor obtained from our treatment is a microscopic quantity that refers to the unit cell. For the bulk, but not 1D or 2D, the electric field $\mathcal{E}$ of the unit cell is the microscopic field which, in general, differs from the displacement field $\mathbf{D}$. Although our implementation includes arbitrary ω_1 and ω_2, for simplicity we present test results primarily for the SHG and Pockels tensor components. Tables II and III show that the variation of these components from the case of one LiF molecule to the bulk through intermediate dimensionalities (cf. Fig. 1) can be reproduced correctly with our implementation of the dynamic CPHF and CPKS schemes. Both tables are divided into four blocks, each corresponding to systems consisting of the same kind of "monomers", either molecules or infinite linear chains or 2D-periodic monolayers. Column N contains the number of "monomers" used to form the finite n-dimensional systems. For example, in the block "molecules", N specifies the number of Li-F units in the corresponding finite linear chain, whereas in the block "slab" it indicates the number of 2D-infinite LiF layers in the stack. $N = 1$ always refers to the proper 0-3D system, which is infinite along 0-3 independent space directions.

For the finite systems, the values reported in Tables II and III are normalized to one Li-F unit in the following manner. The value of each tensor component for $N > 2$ was obtained as half the difference between the result calculated for the system consisting of N "monomers" and that of the system consisting of $N - 2$ "monomers". This procedure tends to remove border effects and accelerates the trend to the corresponding infinite periodic system.

Let us focus first on Table II, which reports the results obtained at the Hartree-Fock level at $\omega = 200$ nm. Starting from the LiF molecule and building oligomers we see the most dramatic changes in the first lines of the table, while the difference from the dynamic hyperpolarizability of the polymer is already reduced to the third significant figure with 15 monomers. It is, however, necessary to build consistently large oligomers—100 molecules—in order to reach convergence to four significant figures. Convergence to the polymer limit is in some cases (xzz and yxy directions) somewhat poorer for the SHG tensor as compared to dc-P, since the former requires solving the CPHF equations at $\omega = 100$ nm which approaches the first resonance (cf. Figure 2).

Similar behavior is found for the buildup from 1D to 2D. Note how some symmetries—i.e., between xyy and xzz—immediately break as soon as just 3 polymers are stacked. As already observed in other cases,[11,25,26] the stacking of slabs to build the 3D periodic bulk shows faster convergence with regard to the number of monomers; the beta values do not change beyond 11 or 13 layers. Equations (B2)-(B5) are here applied (entries with a star) to values of the tensor involving the z direction in order to recover the microscopic quantity as described in the bulk calculation. The above mentioned symmetries are, then, fully restored in the bulk.

Table III reports the same information but obtained at the DFT(B3LYP) level and for a frequency of 300 nm. The choice of a different ω value than for HF was dictated by an earlier

TABLE II. Trend of the dc-Pockels and SHG tensor components from a LiF molecule to bulk LiF (cf. Figure 1), computed at $\omega = 200$ nm, Hartree-Fock. The molecule and linear chains are oriented along x and slabs are parallel to the x-y plane. N denotes the number of molecules used to form a finite linear chain or the number of chains forming a monolayer or the thickness of a slab. Interionic distances are kept constant. Entries with a star correspond to data obtained from the microscopic quantities as discussed in Section III and in Appendix B. All data in atomic units.

		dc-Pockels							Second harmonic generation				
System	N	xxx	xyy	xzz	yxy	yyx	zxz	zzx	xxx	xyy	xzz	$yxy = yyx$	$zxz = zzx$
	1	−6.2120	−2.7794	−2.7794	−4.1157	−2.7794	−4.1157	−2.7794	−20.4391	−1.3726	−1.3729	−40.3110	−40.3081
	3	3.8835	−0.9761	−0.9761	−1.0888	−0.9761	−1.0888	−0.9761	16.1623	−3.4948	−3.4947	−4.3287	−4.3288
	15	7.8542	−0.6686	−0.6686	−0.5028	−0.6686	−0.5029	−0.6686	35.4636	−4.1755	−4.1753	2.4014	2.4003
Molecule	35	7.8931	−0.6649	−0.6650	−0.4960	−0.6649	−0.4961	−0.6650	35.6665	−4.1830	−4.1853	2.4747	2.4752
	50	7.8963	−0.6646	−0.6644	−0.4954	−0.6646	−0.4953	−0.6644	35.6825	−4.1865	−4.1826	2.4816	2.4801
	75	7.8992	−0.6644	−0.6645	−0.4951	−0.6644	−0.4952	−0.6645	35.6950	−4.1846	−4.1858	2.4827	2.4838
	100	7.8995	−0.6642	−0.6643	−0.4948	−0.6642	−0.4949	−0.6643	35.6995	−4.1842	−4.1870	2.4892	2.4874
	1	7.9003	−0.6642	−0.6642	−0.4947	−0.6642	−0.4947	−0.6642	35.7036	−4.1857	−4.1859	2.4899	2.4902
	3	4.8842	−0.4432	−0.1537	−0.3038	−0.4432	−0.1100	−0.1537	20.5484	−4.3378	−0.7606	−2.0717	−0.5404
Polymer	7	5.3244	−0.2838	−0.1771	−0.1263	−0.2838	−0.1165	−0.1771	21.9150	−4.2349	−1.0192	−0.7933	0.2171
	35	5.3240	−0.2955	−0.1726	−0.1277	−0.2955	−0.1137	−0.1726	21.9218	−4.5185	−0.9930	−0.8807	0.2106
	50	5.3240	−0.2967	−0.1722	−0.1281	−0.2967	−0.1135	−0.1722	21.9218	−4.5384	−0.9907	−0.8870	0.2100
	1	5.3238	−0.2994	−0.1713	−0.1294	−0.2994	−0.1129	−0.1713	21.9214	−4.5832	−0.9855	−0.9012	0.2085
	3	3.4278	−0.3589	−0.1567	−0.2748	−0.3589	−0.1150	−0.1567	10.1007	−1.9377	−0.8701	−1.0591	−0.4221
	5	3.5983	−0.3612	−0.1173	−0.2684	−0.3612	−0.0817	−0.1173	10.0036	−2.0000	−0.6465	−0.8491	−0.2060
	7	3.5983	−0.3612	−0.1173	−0.2684	−0.3612	−0.0817	−0.1173	9.9501	−1.9752	−0.6594	−0.8303	−0.2195
Slab	9	3.5855	−0.3567	−0.1240	−0.2640	−0.3567	−0.0883	−0.1240	9.9470	−1.9734	−0.6602	−0.8287	−0.2200
	11	3.5853	−0.3567	−0.1240	−0.2639	−0.3567	−0.0883	−0.1240	9.9467	−1.9732	−0.6602	−0.8286	−0.2201
	11*			−0.3540			−0.2638	−0.3528			−1.9730		−0.8284
	13	3.5853	−0.3566	−0.1240	−0.2639	−0.3566	−0.0883	−0.1240	9.9467	−1.9732	−0.6602	−0.8285	−0.2201
	13*			−0.3540			−0.2639	−0.3529			−1.9730		−0.8285
Bulk		3.5860	−0.3520	−0.3519	−0.2639	−0.3520	−0.2639	−0.3524	9.9522	−1.9708	−1.9737	−0.8155	−0.8150

TABLE III. Same as Table II but for DFT (B3LYP) at 300 nm wavelength.

		dc-Pockels							Second harmonic generation				
System	N	xxx	xyy	xzz	yxy	yyx	zxz	zzx	xxx	xyy	xzz	$yxy = yyx$	$zxz = zzx$
	1	−8.5371	−2.9987	−2.9987	−3.6115	−2.9987	−3.6115	−2.9987	−9.8777	−3.7446	−3.7445	−7.7311	−7.7312
	3	2.4988	−1.5474	−1.5474	−1.8449	−1.5474	−1.8450	−1.5474	3.7311	−2.5948	−2.5948	−5.4923	−5.4924
Molecule	15	12.3042	−0.9134	−0.9134	−0.8482	−0.9134	−0.8481	−0.9134	22.6987	−1.8055	−1.8055	−1.1336	−1.1335
	35	12.3823	−0.9080	−0.9080	−0.8405	−0.9080	−0.8404	−0.9080	22.8466	−1.8000	−1.8000	−1.1125	−1.1122
	50	12.3903	−0.9075	−0.9074	−0.8396	−0.9075	−0.8396	−0.9074	22.8611	−1.7995	−1.7993	−1.1101	−1.1101
	100	12.3956	−0.9069	−0.9072	−0.8390	−0.9069	−0.8392	−0.9072	22.8717	−1.7987	−1.7994	−1.1084	−1.1085
	1	12.3977	−0.9068	−0.9069	−0.8389	−0.9068	−0.8389	−0.9069	22.8755	−1.7991	−1.7991	−1.1077	−1.1077
Polymer	7	8.9257	−1.3979	−0.1997	−1.2777	−1.3979	−0.1720	−0.1997	18.2209	−4.5974	−0.4009	−3.6272	−0.1781
	35	8.9240	−1.5205	−0.1950	−1.3829	−1.5205	−0.1682	−0.1950	18.2174	−5.0528	−0.3910	−3.9442	−0.1754
	50	8.9240	−1.5285	−0.1945	−1.3904	−1.5285	−0.1678	−0.1945	18.2176	−5.0809	−0.3900	−3.9708	−0.1770
	1	8.9250	−1.5474	−0.1935	−1.4084	−1.5476	−0.1669	−0.1935	18.2192	−5.1455	−0.3879	−4.0320	−0.1739
	3	5.3693	−1.0269	−0.4126	−0.9352	−1.0269	−0.3618	−0.4126	10.7419	−2.8748	−1.1669	−2.3447	−0.8110
	5	5.5510	−1.0774	−0.2936	−0.9776	−1.0774	−0.2574	−0.2936	10.0036	−2.0000	−0.6465	−0.8491	−0.2060
	7	5.5378	−1.0689	−0.3040	−0.9697	−1.0689	−0.2678	−0.3040	10.0750	−2.8095	−0.7767	−2.1754	−0.5270
Slab	9	5.5359	−1.0679	−0.3048	−0.9687	−1.0679	−0.2685	−0.3048	10.0716	−2.8067	−0.7778	−2.1730	−0.5279
	11	5.5358	−1.0677	−0.3048	−0.9686	−1.0677	−0.2685	−0.3048	10.0713	−2.8064	−0.7778	−2.1727	−0.5280
	11*			−1.0679			−0.9688	−1.0679			−2.8065		−2.1731
	13	5.5357	−1.0678	−0.3048	−0.9686	−1.0678	−0.2685	−0.3048	10.0713	−2.8064	−0.7779	−2.1727	−0.5280
	13*			−1.0680			−0.9688	−1.0680			−2.8066		−2.1731
Bulk		5.5434	−1.0663	−1.0662	−0.9701	−1.0663	−0.9701	−1.0661	10.0829	−2.8133	−2.8138	−2.1692	−2.1689

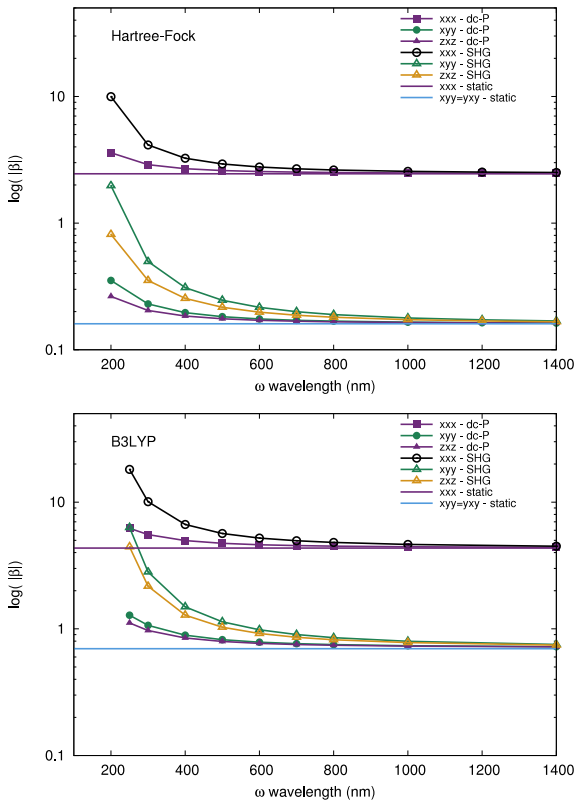

FIG. 2. Dependence of symmetry-independent dc-Pockels (dc-P) ($\beta(0,\omega,-\omega)$) and SHG tensor elements $\beta(\omega,\omega,-2\omega)$ of bulk LiF on the ω wavelength and their convergence to the static limit. The LiF bulk structure is slightly distorted as described in Section III B 1. Calculations at the HF level (top panel) and B3LYP (bottom panel).

occurrence of the first resonance in the DFT case (*vide infra*). All conclusions drawn above for the HF case are valid here as well, thus validating the correctness of the dynamic CPKS hyperpolarizability implementation.

Overall, we believe this extensive test provides a robust proof of the validity of the equations and their implementation, although we note that the numerical precision is somewhat less good than for the static β case (see Ref. 11). This is essentially to be ascribed to the above-mentioned instability in the convergence of the dynamic CPHF/KS procedure as one approaches a resonance. Note that the values adopted for ω represent fairly high frequencies, not far from the resonance in the SHG case, which we chose with the precise purpose to heavily stress the code.

C. Convergence to the static values

A necessary condition for the correctness of the $\beta(-\omega_\sigma;\omega_1,\omega_2)$ tensor is that, for both dc-P and SHG (and, of course, also in the general case), all the values converge to the static hyperpolarizability at low frequency. In Figure 2, some symmetry-independent values are reported for the bulk LiF structures as described in Sec. III B 1, for Hartree-Fock (top panel) and B3LYP (bottom panel).

The convergence to the static case is evident. In addition, we note that the B3LYP values are 3 to 6 times larger at 250 nm with respect to the corresponding Hartree-Fock ones, indicating an earlier occurrence of the first resonance—as a matter of fact, we were not able to converge the first order coupled perturbed iterations at ω = 100 nm, needed to compute SHG at ω = 200 nm.

D. Connection between Pockels and SHG

Almost 20 years ago, Bishop and De Kee[23,24] derived dispersion relations for the diagonal components of electronic hyperpolarizabilities. Restricting ourselves to the quantities of interest in the present work (first hyperpolarizabilities), and to the xxx component, their expression reads

$$\beta_{xxx}(-\omega_\sigma;\omega_1,\omega_2) = \beta_{xxx}(0;0,0) + A\,W_2 + B\,W_2^2 + B'\,W_4 + \cdots \qquad (9)$$

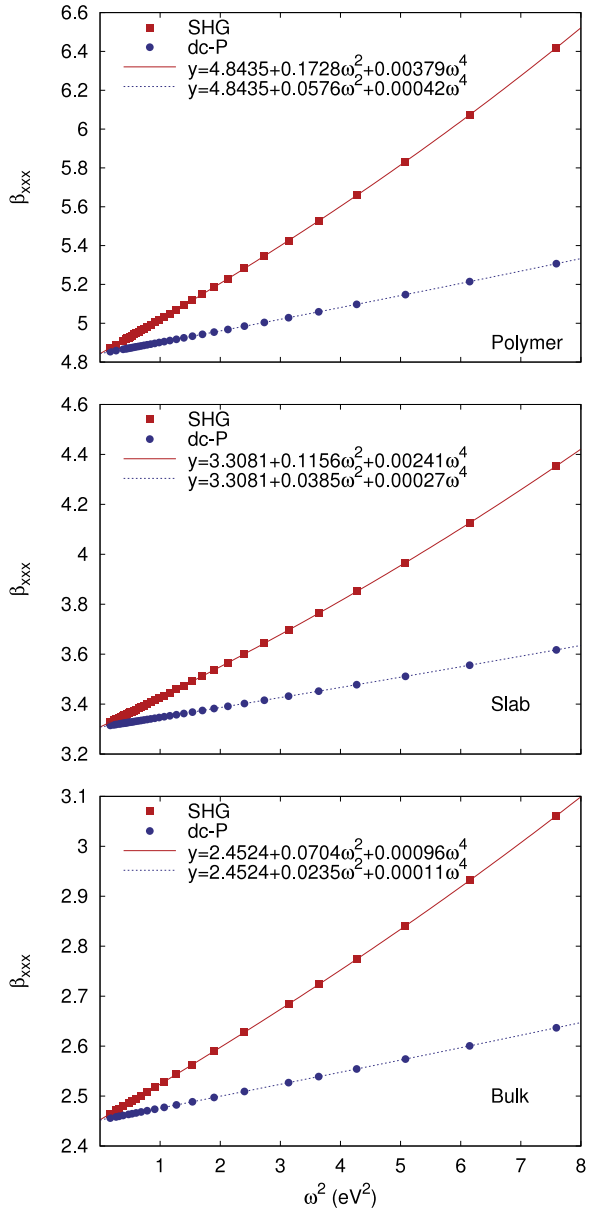

FIG. 3. Polynomial fit of the β_{xxx} element of the SHG and Pockels tensors of the 1D polymer (top panel), 2D slab (middle panel), and 3D bulk (bottom panel) distorted LiF structures.

with $W_2 = \omega_\sigma^2 + \omega_1^2 + \omega_2^2$ and $W_4 = \omega_\sigma^4 + \omega_1^4 + \omega_2^4$. The coefficients A, B, and B′ are independent of the optical frequencies ω_1 and ω_2. For SHG and dc-P, the frequency ratios are

$$\frac{W_2^{SHG}}{W_2^{dc\text{-}P}} = 3, \tag{10}$$

$$\frac{W_4^{SHG}}{W_4^{dc\text{-}P}} = \frac{(W_2^{SHG})^2}{(W_2^{dc\text{-}P})^2} = 9. \tag{11}$$

In order to verify that the $\beta_{xxx}(-\omega_\sigma;\omega_1,\omega_2)$ computed with our method for periodic systems satisfies the above relations, we computed the SHG and dc-P β_{xxx} for a number of frequencies and fit the results to the polynomial $y = a + bx + cx^2 + dx^3$ with $x = \omega^2$. The range [0:7] eV^2 for ω^2 was selected as reasonably far from the first resonance, but wide enough to exploit the quartic term (in ω). We have found it important to have a dense sampling of ω^2 to have good numerical accuracy in the fit. The computed points and fitting polynomials are shown in Figure 3. Obviously, the ideal SHG/dc-P ratios for b and c in the fitting polynomial are 3 and 9, respectively. These ratios are reported in Table IV for 1-3D where excellent agreement with the ideal values is seen.

IV. MOLYBDENUM DISULFIDE

MoS_2 molybdenite is the most important ore of the metal molybdenum and its natural crystals are commonly found in hydrothermal deposits. Recently, interest in this long-known material has risen alongside other two-dimensional materials like graphene[30] and hexagonal BN, because of the ability of MoS_2 to form single-layer and few-layer structures with widely varying properties.

In this context, SHG measurements represent a powerful experimental tool to discern the number of layers present in MoS_2 2D structures. For an even number of layers, the structure is nearly centro-symmetric, but for an odd number it is not and, therefore, is expected to exhibit significant SHG. As reported by several authors,[31,32] the monolayer shows a very high SHG response, which is strongly attenuated with an increasing (odd) number of layers. In the SHG tensor of such structures, the only nonvanishing components are $\beta_{yyy} = -\beta_{yxx} = -\beta_{xxy} = -\beta_{xyx}$. Thanks to the strong anisotropic character of this tensor, SHG microscopy is also used to measure accurately the orientation of the material with respect to the laser beam.

Despite the large interest in MoS_2, including a number of experimental works,[33] only few theoretical papers can be found[34–36] and no simulation of NLO properties. We have computed the SHG tensor of 1–5 odd layer MoS_2 at ω = 810 nm (the Ti:sapphire laser wavelength used in Refs. 31 and 32). The dispersion-corrected hybrid functional B3LYP-D2, with rescaled factors in the dispersion correction as suggested by Civalleri *et al.*,[37] was adopted for this purpose. All structures were cut out from the bulk and, then, fully optimized (cell parameters and atomic positions). An all-electron Gaussian type basis set was used for S,[38] (8s)(6311sp)(1d), with the lowest sp exponent re-optimized to 0.1506 bohr^{-2}. For Mo, we employed a HAYWSC-(311sp)(31d)[39] basis set, incorporating the Hay and Wadt small core pseudopotential[40] for core electrons and Gaussian type functions for valence shells.

The computed β_{yyy} values for the mono-, tri-, and pentalayer are 49 025, 6434, and 1709, respectively. Values are in atomic units, per unit cell and normalized for the number of layers. These values are also reported in Figure 4. We note that the strong dependence of SHG tensors on the thickness of the slab mentioned above is reproduced. In Ref. 31 it is stated that "$\chi^{(2)}$ of the trilayer is about a factor of seven smaller than the monolayer, while those of the bilayer and quadralayer are about two orders of magnitude smaller than the monolayer." We find our results above in line with this experimental observation: $\beta_{yyy}^{1L}/\beta_{yyy}^{3L} = 7.6$. Our results are also in line with the findings of Li *et al.*,[32] where this ratio is found to be ≈6.0 ± 0.5 (obtained from square root of SHG intensity data in Figure 4 of Ref. 32, normalized by the number of layers). From the same article, the estimated ratio between the monolayer and the pentalayer is $\beta_{yyy}^{1L}/\beta_{yyy}^{5L} \approx 14 \pm 1$, which differs by a factor of 2 from our estimate (=28). We consider that to be good agreement since the small SHG value of the pentalayer implies fairly large error limits. The pentalayer was not investigated in Ref. 31. As a side note, we report that the corresponding computed static values, normalized for the number of layers, are (in a.u.): $\beta_{yyy}^{1L} = 1014$, $\beta_{yyy}^{3L} = 320$, $\beta_{yyy}^{5L} = 194$.

We also carried out calculations on the nearly symmetric bilayer and quadralayer, in which case we find, within the numerical accuracy of the algorithm, null tensor elements. In fact, thermal effects and defects in real systems can play a significant role in breaking the symmetry, thus allowing for an enhanced SHG response in slabs with an even number of layers.

TABLE IV. Check of the Bishop-De Kee dispersion formula (cf. Eq. (9)) from a polynomial fit of the data in Figure 3. *b* and *c* refer to the coefficients of the linear and quadratic term of the polynomial in ω^2, respectively. Ideal values are 3 for $b^{SHG}/b^{dc\text{-}P}$ and 9 for $c^{SHG}/c^{dc\text{-}P}$.

	Polymer	Slab	Bulk
$b^{SHG}/b^{dc\text{-}P}$	2.999	3.001	3.000
$c^{SHG}/c^{dc\text{-}P}$	9.042	9.041	9.128

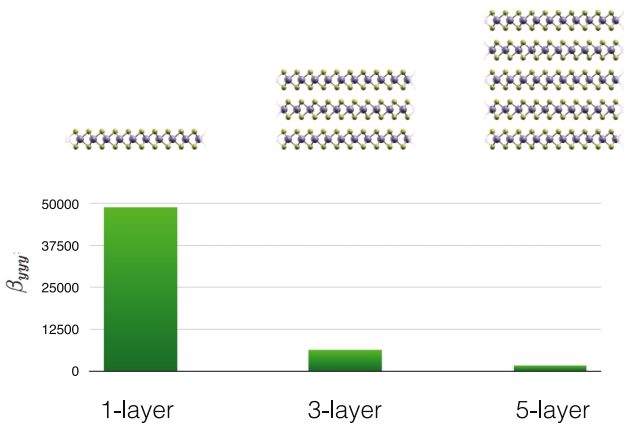

FIG. 4. Layer dependence of the computed (B3LYP) SHG β_{yyy} tensor component (in atomic units, normalized for the number of layers) for few-layer MoS_2 structures, at ω = 810 nm.

This preliminary investigation shows the applicability of our approach to systems of technological interest and paves the way for relating the electronic structure to SHG and other NLO properties. In the future, we plan to undertake a more complete investigation of the role of different Hamiltonians and basis sets on both the structure and response properties.

V. CONCLUSIONS

An analytical CPHF/CPKS method for computing the frequency-dependent electronic first hyperpolarizability $\beta(-\omega_\sigma,\omega_1,\omega_2)$ tensor of periodic systems in 1, 2, and 3D has been implemented in the CRYSTAL code. Various tests have been carried out, with SHG and the dc-P effect as examples, that confirm the correctness and accuracy of our implementation. These tests include a build-up from 0D to 3D using LiF as a model system. We also verified symmetry requirements, convergence to the static limit, and the Bishop-deKee dispersion formula relating dc-P and SHG.

Preliminary SHG calculations on multi-layer structures of the technologically important material MoS_2 satisfactorily reproduce experimental data and, thereby, pave the way for future understanding of the structure property relationship in that case as well as predicting NLO properties of other potentially interesting non-centrosymmetric systems.[42]

APPENDIX A: ω-FIELD FREQUENCY DEPENDENCE OF $I\frac{\partial U^v_{ai(+\omega_2)}(\vec{k})}{\partial k_u}$

An expression for $\partial U^v_{ai}(\vec{k})/\partial k_u$ is derived in Appendix A of Ref. 7 for 1D periodic systems, which is readily generalized to 3D. It is convenient to write the result in terms of the Q matrix defined by

$$\frac{\partial C_{\mu p}(\vec{k})}{\partial k_u} = \sum_q^{\text{all}} C_{\mu q}(\vec{k}) Q^u_{qp}(\vec{k}) \tag{A1}$$

where, for $p \neq q$ (p and q will denote, here and in the following, general orbitals, either occupied or virtual), $Q^u(\vec{k})$ elements are[41]

$$Q^u_{pq}(\vec{k}) = \frac{F^{k_u}_{pq}(\vec{k}) - R^{k_u}_{pq}(\vec{k}) E_q(\vec{k})}{\mathbb{E}_q(\vec{k}) - \mathbb{E}_p(\vec{k})}, \tag{A2}$$

where we have defined

$$F^{k_v}_{pq}(\vec{k}) = \sum_{\mu,\nu} C^*_{\mu p}(\vec{k}) \frac{\partial F_{\mu\nu}(\vec{k})}{\partial k_v} C_{\nu q}(\vec{k}), \tag{A3}$$

$$R^{k_v}_{pq}(\vec{k}) = \sum_{\mu,\nu} C^*_{\mu p}(\vec{k}) \frac{\partial S_{\mu\nu}(\vec{k})}{\partial k_v} C_{\nu q}(\vec{k}). \tag{A4}$$

Then, using $F^{(v)}_{(+\omega_2)}$ as the perturbed Fock matrix for the ω_2 field, we have

$$\frac{\partial U^{(v)}_{ai(+\omega_2)}(\vec{k})}{\partial k_u} = \frac{\frac{\partial}{\partial k_u} G^{(v)}_{ai(+\omega_2)}(\vec{k})}{\mathbb{E}_i(\vec{k}) - \mathbb{E}_a(\vec{k}) - \omega_2} - \frac{G^{(v)}_{ai(+\omega_2)}(\vec{k}) \frac{\partial}{\partial k_u} \left(\mathbb{E}_i(\vec{k}) - \mathbb{E}_a(\vec{k})\right)}{\left(\mathbb{E}_i(\vec{k}) - \mathbb{E}_a(\vec{k}) - \omega_2\right)^2}, \tag{A5}$$

where

$$\frac{\partial G^{(v)}_{ai(+\omega_2)}(\vec{k})}{\partial k_u} = \sum_p^{all} \left(Q^u_{pa}(\vec{k})\right)^* G^{(v)}_{pi(+\omega_2)}(\vec{k}) + \sum_p^{all} G^{(v)}_{ap(+\omega_2)}(\vec{k}) Q^u_{pi}(\vec{k}) + \sum_{\mu,\nu} C^*_{\mu p}(\vec{k}) \frac{\partial F^{(v)}_{\mu\nu(+\omega_2)}(\vec{k})}{\partial k_u} C_{\nu q}(\vec{k}). \tag{A6}$$

The evaluation of the last term on the r.h.s. of Eq. (A6) is straightforward except for the term $\frac{\partial Q^v_{pq}}{\partial k_u}$ contained in it. This term, however, does not depend on the ω_2 frequency, and can be thus computed as in the static case.[10,43]

APPENDIX B: FROM DYNAMIC (HYPER)POLARIZABILITIES TO ELECTRIC SUSCEPTIBILITIES

The α and β tensors obtained from our CPHF treatment are microscopic quantities that refer to a unit cell in the case of polymers, slabs, and crystals (and to a single molecule in the 0D case). Thus, the electric field $\mathcal{E}$ is the macroscopic field felt by the unit cell in the bulk, and in general, differs from **D**, the displacement field,[44] according to the following equation (in a.u.):

$$\begin{aligned} D_a &= \mathcal{E}_a + 4\pi P_a \\ &= \mathcal{E}_a + \textstyle\sum_b \chi^{(1)}_{ab} \mathcal{E}_b + \sum_{b,c} \chi^{(2)}_{abc} \mathcal{E}_b \mathcal{E}_c + \cdots \\ &= \textstyle\sum_b \epsilon_{ab} \mathcal{E}_b, \end{aligned} \tag{B1}$$

where $\epsilon_{ab} = \delta_{ab} + \chi^{(1)}_{ab}$ is the dielectric constant (at zeroth-order of perturbation), $\chi^{(2)}$ the nonlinear susceptibility, and **P** is the polarization vector, which is the induced dipole moment per unit volume. If the indices of the tensor component of interest correspond to mixed periodic and non-periodic directions, as for the slab, $D_a/\mathcal{E}_a \simeq 1$ (periodic direction) or $D_b/\mathcal{E}_b \simeq \epsilon^{[0]}_{bb}$ (non-periodic direction) must be used according to the periodicity of the a and b directions used. Following the same demonstration as in Ref. 18 but for the Pockels and SHG susceptibilities of LiF slab, we find

$$\chi^{(2)}_{xzz}(-\omega;\omega,0) = \chi^{(2)}_{zxz}(-\omega;\omega,0) = \frac{2\pi}{V}\beta_{xzz}(-\omega;\omega,0)\epsilon_{zz}(\omega)\epsilon_{zz}(0), \tag{B2}$$

$$\chi^{(2)}_{zzx}(-\omega;\omega,0) = \frac{2\pi}{V}\beta_{zzx}(-\omega;\omega,0)\epsilon_{zz}(\omega)^2, \tag{B3}$$

$$\chi^{(2)}_{xzz}(-2\omega;\omega,\omega) = \frac{2\pi}{V}\beta_{xzz}(-2\omega;\omega,\omega)\epsilon_{zz}(\omega)^2, \tag{B4}$$

$$\chi^{(2)}_{zzx}(-2\omega;\omega,\omega) = \chi^{(2)}_{zxz}(-2\omega;\omega,\omega) = \frac{2\pi}{V}\beta_{zzx}(-2\omega;\omega,\omega)\epsilon_{zz}(2\omega)\epsilon_{zz}(\omega). \tag{B5}$$

[1]R. W. Boyd, *Nonlinear Optics*, 3rd ed. (Academic Press, Elsevier, 2008).
[2]R. A. Ganeev, *Nonlinear Optical Properties of Materials*, Springer Series in Optical Sciences (Springer, 2013).
[3]F. L. Gu, Y. Aoki, M. Springborg, and B. Kirtman, in *Calculations on Nonlinear Optical Properties for Large Systems. The Elongation Method*,

Springer Briefs in Molecular Science, Electrical and Magnetic Properties of Atoms, Molecules, and Clusters, edited by G. Maroulis (Springer, 2015).
[4]P. N. Butcher and D. Cotter, *The Elements of Nonlinear Optics* (Cambridge University Press, 1991).
[5]R. Resta, Rev. Mod. Phys. **66**, 899 (1994).
[6]R. D. King-Smith and D. Vanderbilt, Phys. Rev. B **47**, 1651 (1993).
[7]B. Kirtman, F. L. Gu, and D. M. Bishop, J. Chem. Phys. **113**, 1294 (2000).
[8]P. Otto, F. L. Gu, and J. Ladik, J. Chem. Phys. **110**, 2717 (1999).
[9]M. Springborg and B. Kirtman, Phys. Rev. B **77**, 045102 (2008).
[10]M. Ferrero, M. Rérat, R. Orlando, and R. Dovesi, J. Comput. Chem. **29**, 1450 (2008).
[11]M. Ferrero, M. Rérat, R. Orlando, and R. Dovesi, J. Chem. Phys. **128**, 014110 (2008).
[12]R. Dovesi, V. R. Saunders, C. Roetti, R. Orlando, C. M. Zicovich-Wilson, F. Pascale, B. Civalleri, K. Doll, N. M. Harrison, I. J. Bush, P. D'Arco, M. Llunell, M. Causà, and Y. Noël, CRYSTAL14 User's Manual, University of Torino, 2014.
[13]R. Dovesi, R. Orlando, C. M. Zicovich-Wilson, B. Civalleri, L. Maschio, A. Erba, S. Casassa, M. Ferrabone, M. D. L. Pierre, P. D'Arco, Y. Noël, M. Causà, M. Rérat, and B. Kirtman, Int. J. Quantum Chem. **114**, 1287 (2014).
[14]R. Orlando, R. Bast, K. Ruud, U. Ekström, M. Ferrabone, B. Kirtman, and R. Dovesi, J. Phys. Chem. A **115**, 12631 (2009).
[15]R. Orlando, V. Lacivita, R. Bast, and K. Ruud, J. Chem. Phys. **132**, 244106 (2010).
[16]R. Dovesi, Int. J. Quantum Chem. **29**, 1755 (1986).
[17]T. Seidler, K. Stadnicka, and B. Champagne, J. Chem. Theory Comput. **10**, 2114 (2014).
[18]M. Ferrero, M. Rérat, B. Kirtman, and R. Dovesi, J. Chem. Phys. **129**, 244110 (2008).
[19]S. P. Karna and M. Dupuis, J. Comput. Chem. **12**, 487 (1991).
[20]D. M. Bishop, J. Chem. Phys. **100**, 6535 (1994).
[21]B. J. Orr and J. F. Ward, Mol. Phys. **20**, 513 (1971).
[22]P. Otto, Phys. Rev. B **45**, 10876 (1992).
[23]D. M. Bishop and D. W. De Kee, J. Chem. Phys. **104**, 9876 (1996).
[24]D. M. Bishop and D. W. De Kee, J. Chem. Phys. **105**, 8247 (1996).
[25]L. Maschio, B. Kirtman, R. Orlando, and M. Rérat, J. Chem. Phys. **137**, 204113 (2012).
[26]L. Maschio, B. Kirtman, M. Rérat, R. Orlando, and R. Dovesi, J. Chem. Phys. **139**, 164102 (2013).
[27]M. Ferrero, M. Rérat, R. Orlando, R. Dovesi, and I. Bush, in *In Ab Initio Simulation of Crystalline Solids: History and Prospects*, edited by R. Dovesi, C. Roetti, and R. Orlando (IOP Publishing, Bristol, UK, 2008), Vol. 117, p. 012026.
[28]P. Pulay, J. Comput. Chem. **3**, 556 (1982).
[29]A. J. Garza and G. E. Scuseria, J. Chem. Phys. **137**, 054110 (2012).
[30]A. K. Geim and K. S. Novoselov, Nat. Mater. **6**, 183 (2007).
[31]N. Kumar, S. Najmaei, Q. Cui, F. Ceballos, P. M. Ajayan, J. Lou, and H. Zhao, Phys. Rev. B **87**, 161403 (2013).
[32]Y. Li, Y. Rao, K. F. Mak, Y. You, S. Wang, C. R. Dean, and T. F. Heinz, Nano Lett. **13**, 3329 (2013).
[33]Q. H. Wang, K. Kalantar-Zadeh, A. Kis, J. N. Coleman, and M. S. Strano, Nat. Nanotechnol. **7**, 699–712 (2012).
[34]S. Lebègue and O. Eriksson, Phys. Rev. B **79**, 115409 (2009).
[35]A. Kumar and P. Ahluwalia, Eur. Phys. J. B **85**, 186 (2012).
[36]S. Ahmad and S. Mukherjee, Graphene **3**, 52 (2014).
[37]B. Civalleri, C. Zicovich-Wilson, L. Valenzano, and P. Ugliengo, CrystEngComm **10**, 405 (2008).
[38]A. Lichanot, E. Aprà, and R. Dovesi, Phys. Status Solidi B **177**, 157 (1993).
[39]F. C. A. Patel, N. M. Harrison, C. Roetti, and C. R. A. Catlow, J. Mater. Chem. **7**, 959 (1997).
[40]W. R. Wadt and P. J. Hay, J. Chem. Phys. **82**, 284 (1985).
[41]In the case where p and q are degenerated (their eigenvalue difference is less than 10^{-12} hartree), they are separated by 10^{-12} hartree to avoid a 0 over 0 calculation of the real part of $Q^u(\vec{k})$.
[42]M. Rérat, L. Maschio, B. Kirtman, B. Civalleri, and R. Dovesi, J. Chem. Theory Comput. (2015) (in press).
[43]D. M. Bishop, F. L. Gu, and B. Kirtman, J. Chem. Phys. **114**, 7633 (2001).
[44]N. W. Ashcroft and N. D. Mermin, *Solid State Physics* (Holt-Saunders International Editions, Weinheim, 1976).